IIETA International Information and Engineering Technology Association
Advancing the World of Information and Engineering

Journal Européen des Systèmes Automatisés
Vol. 59, No. 5, May, 2026, pp. 1207-1224
Journal homepage: http://iieta.org/journals/jesa

Optimization and Feasibility Analysis of Grid-Connected Photovoltaic Systems for Zero-Energy Housing in Algeria

Zoubida Alliche[1*], Fadhela Fodhil[2], Redha Bendoumia[1], Leila Berkani[1]

[1] Department of Electronics, Faculty of Technology, University of Blida 1, Blida 09000, Algeria
[2] Department of Rural Engineering, National Higher School of Agronomy, Algiers 16004, Algeria

Corresponding Author Email: zoubida_alliche@univ-blida.dz

https://doi.org/10.18280/jesa.590503

Received: 5 March 2026
Revised: 11 May 2026
Accepted: 20 May 2026
Available online: 31 May 2026

Keywords:
zero-energy house, grid-connected photovoltaic system, electric vehicle, feasibility assessment, water cycle–moth flame optimization algorithm

ABSTRACT

This study investigates the feasibility of a zero-energy house (ZEH) in northern Algeria, integrating a grid-connected photovoltaic (PV) system and an electric vehicle (EV). The optimal system performance is assessed using the Water Cycle–Moth Flame Optimization (WCAMFO) algorithm under two load profiles, considering cases with and without EV integration. The optimization objective is to minimize the net present cost (NPC) while satisfying constraints related to the renewable fraction (RF), rooftop area, and the zero-energy balance. Two scenarios are analyzed to evaluate the technical, economic, and environmental impacts on the ZEH. The proposed approach is benchmarked against Hybrid Optimization Model for Electric Renewables (HOMER) software in terms of NPC, cost of electricity (COE), and RF. The results show that WCAMFO consistently outperforms HOMER across all configurations. For the base load case, the optimal solution consists of a 2.28 kWp PV system and a 2.5 kW converter, achieving RF values of 69% and 82.6% with negative COE values, indicating economic viability. EV integration increases energy demand, reducing RF to 33.4% and 36.86%. However, by optimally integrating the EV load while enforcing the zero-energy constraint and maintaining RF above 50%, a positive energy balance is preserved. These findings contribute to Algeria's sustainable energy transition by presenting practical and cost-effective solutions.

1. INTRODUCTION

Since 1995, Algeria has witnessed an annual increase of about 2% in global greenhouse gas (GHG) emissions [1], and the North African country ranks as Africa's third-largest emitter of carbon dioxide (CO_2), with a marginal increase of around 4.4% in air pollution, which was recorded, corresponding to 169.2 MT of CO_2 emissions in 2019 [2].

Therefore, the country has adopted sustainable green energy policies and promoted energy efficiency with the objective of limiting GHG emissions and alleviating climate change impacts. To align with the national sustainable development strategy, Algeria has been actively implementing and updating various renewable energy programs and strategies [3]. One major objective of these initiatives is to achieve a 7% reduction in GHG emissions by 2030 [4]. As part of this effort, photovoltaic (PV) energy stands out as the predominant renewable energy resource in Algeria's clean strategy [5, 6].

The Algerian residential sector accounts for over 44% of the national energy consumption [7], making it responsible for more than one-third of the overall GHG emissions [8, 9]. Thus, this sector has been the target of many programs and actions to raise awareness, measure energy use, and promote energy efficiency [10]. However, to address these challenges, more sustainable energy solutions are required. One promising approach is the uptake of hybrid systems combining renewable energy sources and grid-connected systems, particularly suited for residential and urban environments [11-14] and for net-zero-energy house (net-ZEH) status (homes that achieve energy self-sufficiency by generating as much energy as they use each year).

Various studies have investigated the operation, control, and optimization of hybrid PV grid-connected energy systems. For instance, Chakir et al. [15] proposed a multi-level energy management strategy for a PV/wind/battery energy system to supply five Moroccan households. The recommended system could control the energy made by hybrid renewable energy sources (HRESs) and reduce the amount of energy that needs to be purchased from the utility grid. In this literature [16], a genetic algorithm (GA)-based optimization technique was proposed to optimize a PV/wind/biomass grid-connected system using the lowest cost criteria and a lifecycle perspective. The study revealed that the hybrid system contributes positively to energy autonomy, environmental quality improvement, and job creation. Similarly, Falama et al. [17] optimized and studied four hybrid backup grid-connected systems under severe power outages using dual-objective optimization applied through the firefly algorithm. According to the findings, the on-grid PV battery was more cost-effective than the grid without blackouts. Additionally, Dalton et al.

[18] investigated the techno-financial feasibility of various configurations of grid and renewable energy hybrid systems to power a large-scale grid-connected hotel. Wind energy systems demonstrated their economic viability as the most feasible technology for this application. The authors in this study [19] intended to optimize a PV grid-connected system using Hybrid Optimization Model for Electric Renewables (HOMER) software under four typical climate zones in Queensland, Australia, and discovered that the PV grid system is an efficient solution to curtail electricity bills and offset carbon dioxide emissions. In this study [20], the optimal design of a PV grid energy system for Makkah, Saudi Arabia, was determined using HOMER software, considering the net present cost (NPC), excess electricity, renewable fraction (RF), and CO_2 emissions. In this study [21], an optimal cost-effective system was addressed using a clonal selection algorithm and a GA, where neural forecasting was applied to predict the use of renewable energy sources and load demand fluctuations. In relevant research, González et al. [22] proposed optimizing hybrid grid-connected PV/wind energy systems incorporating real-time, hour-by-hour wind and solar irradiation measurements and local energy usage based on the lowest life cycle cost. Sensitivity analysis was also performed. In study [23], the authors optimized the sizing of a residential grid-connected PV-battery system using a GA.

A time-series simulation of the hybrid system was performed to curtail the yearly electricity cost by adjusting the battery charge and discharge cycles.

Numerous research endeavors have delved into the ideal configuration of hybrid energy systems, with several of them utilizing optimization tools like HOMER [24-27], Retscreen [28, 29] and iHOGA [30-32]. Other studies have focused on other methods and approaches, like linear programming (LP) [33, 34], mixed-integer linear programming (MILP) [35, 36], stochastic programming [37, 38], dynamic programming [39, 40], robust optimization [41, 42], and metaheuristic methods, which are commonly utilized to address the optimal configuration of HRESs. Recently, several algorithms have been widely implemented and proposed, including GA [43-45], particle swarm optimization algorithm (PSO) [26, 46, 47], gray wolf optimizer (GWO) [48-50], cuckoo search algorithm (CSA) [51, 52], salp swarm optimization (SSO) [53, 54], bee colony algorithm (BCA) [55, 56], and whale optimization algorithm (WOA) [57]. These contributions clearly demonstrate the robustness and efficiency of modern optimization algorithms, particularly metaheuristic approaches, in addressing the complexity and sustainability challenges of hybrid renewable energy systems.

More recently, machine learning–based approaches have been introduced for energy optimization and management in hybrid energy systems. Techniques such as artificial neural networks [58, 59], support vector machines [60, 61], and reinforcement learning [62, 63] have been employed for load forecasting, renewable generation prediction, and adaptive energy management strategies. These data-driven methods are particularly effective in handling uncertainty and system nonlinearity. However, their reliance on large datasets and higher computational complexity may limit their applicability in practical grid-connected PV systems without storage, motivating the continued use of deterministic and rule-based optimization approaches as adopted in this study.

In recent years, ZEHs characterized by low energy demand [64] have received increased attention because of numerous benefits, including cost-effectiveness, sustainability, and eco-friendliness [65-68].

In particular, various studies have examined different aspects of ZEHs in the Algerian context [69-71].

For example, Missoum et al. [13] studied how well a solar-heated bioclimatic house performed energetically and explored the possibility of converting it into a ZEH by integrating a grid-connected PV system. The findings indicated that achieving ZEH status for a bioclimatic house using this approach was highly feasible. However, the return on investment would be considerably impacted by the expensive nature of solar energy systems' elements and the comparatively lower costs of conventional energy sources in Algeria. The microeconomic advantages of energy efficiency for a single-family home were evaluated by Ringel et al. [72] in two smart-home scenarios conducted in Algeria and Germany, respectively. Similarly, Laib et al. [73] assessed the efficiency of a grid-connected solar system and the energy balance of a residential building, and implementing energy-saving measures and integrating a grid-connected PV system resulted in a positive annual electricity balance. Mokhtara et al. [74] explored how variations in climate and building energy performance influence the optimization of hybrid renewable energy systems (HRESs) that integrate diesel-based electricity generation to satisfy the energy demands of both low- and high-performance residential structures. The researchers employed a multi-criteria spatial analysis approach to establish a renewable energy potential mapping framework for Algeria. In addition, they used PSO and ε-constraint methods to handle the multi-objective aspects of the problem. The findings revealed that low-efficiency buildings were the optimal configuration for Tindouf and Adrar, whereas high-performance buildings were the best configuration for Biskra and Tamenrasset regions. In a previous study [75], the authors explored the effectiveness of hybrid renewable energy system integration in reaching nearly zero-energy building standards across the Mediterranean area. The performance of three specific systems was evaluated: the underground tank (UNT), the earth-air heat exchanger (EAHE), and the solar thermal collector. The study found that combining the three systems effectively satisfied the residential space heating requirements in Oran, Algeria, with a coverage rate of 131%.

This research contributes to Algeria's national renewable energy objectives by focusing on residential ZEHs as a potential pathway to achieve these goals. The study offers the following contributions:

(i) Analyzing the feasibility, from both technical and economic perspectives, of integrating grid-connected PV systems and EVs into residential ZEHs in Algeria.

(ii) Demonstrating the benefits of using the Water Cycle–Moth Flame Optimization (WCAMFO) algorithm for optimizing hybrid energy systems, with improved accuracy and efficiency when compared to conventional methods like HOMER software.

(iii) Conducting a comprehensive sensitivity analysis to evaluate how factors such as load consumption, RF, and PV system capacity influence the overall system performance.

(iv) Examining the impact of local environmental conditions, feed-in-tariff (FIT) policies, and the integration of EVs on energy balance, RF, and economic feasibility for residential ZEHs in Algeria.

The layout of the paper is presented as follows: Section 2 details the methodology adopted in the study and describes the materials, methods, and proposed approach. Section 3 provides an overview of the case study, while Section 4

focuses on the discussion and analysis of the results. Lastly, concluding remarks summarize the main findings.

2. MATERIALS AND METHODS

2.1 Methodology

This paper evaluates the impact of electric vehicle (EV) integration on a residential load profile in northern Algeria. A novel approach is suggested to optimize the grid-connected PV system in a ZEH using the WCAMFO algorithm. The proposed approach relies on the standard electric load profile of an Algerian household with and without EV integration. Considering two energy scenarios, an optimization analysis is first performed to select the best design of the grid-connected PV system components based on the FIT schemes implemented in Algeria. Figure 1 illustrates the fundamental schematic of the system.

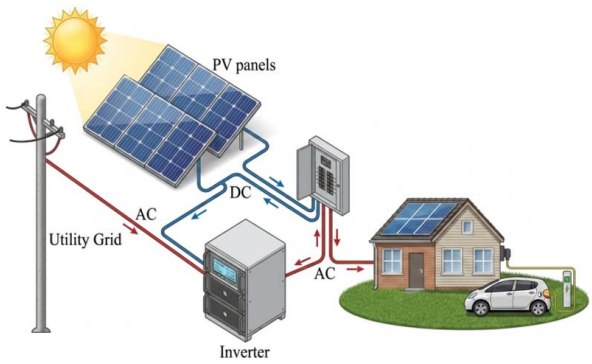

Figure 1. Fundamental schematic of a photovoltaic (PV) grid-connected system

The optimization process prioritizes minimizing NPC and cost of electricity (COE) while adhering to constraints such as the RF, ZEH requirement, and available roof space. The performance of the proposed WCAMFO-based optimization is compared to that of HOMER software to assess their relative effectiveness. Additionally, a sensitivity analysis explores the influence of load consumption, RF, available roof area, ZEH constraints, and PV capacity on the configuration of the optimal hybrid energy system.

2.2 Proposed approach

This study uses a hybrid metaheuristic method called WCAMFO. Introduced by Khalilpourazari and Khalilpourazary [76], the WCAMFO algorithm combined the strengths of two existing algorithms: the water cycle algorithm (WCA) and moth flame optimization (MFO). By merging these two algorithms, the WCAMFO algorithm enhanced performance in the exploration and exploitation phases.

2.2.1 Water cycle algorithm

The WCA represents a nature-inspired optimization method introduced by Eskandar et al. [77] in 2012. Taking inspiration from the natural movement of water in ecosystems, this metaheuristic approach models how streams and rivers converge toward the sea to address constrained optimization problems [78, 79]. The optimization process of the WCA is illustrated in Figure 2.

s

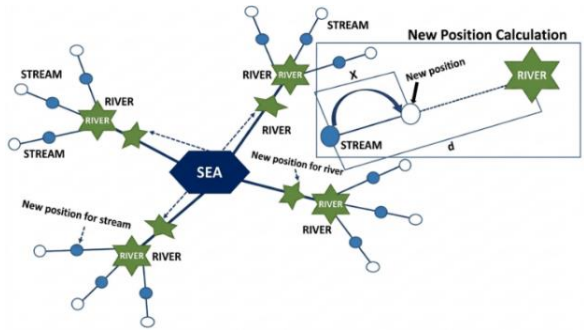

Figure 2. Water cycle algorithm (WCA) optimization process

An initial stream matrix is generated with dimensions $N_p \times D$, where N_p represents the population size and D denotes the total number of variables in the system [77].

$$\text{Total population} = \begin{bmatrix} \text{Sea} \\ \text{River}_1 \\ \text{River}_2 \\ \text{River}_3 \\ \vdots \\ \text{Stream}_{N_{sr}+1} \\ \text{Stream}_{N_{sr}+2} \\ \text{Stream}_{N_{sr}+3} \\ \vdots \\ \text{Stream}_{N_p} \end{bmatrix} = \begin{bmatrix} x_1^1 & x_2^1 & x_3^1 & \dots & x_D^1 \\ x_1^2 & x_2^2 & x_3^2 & \dots & x_D^2 \\ \vdots & \vdots & \vdots & \vdots & \vdots \\ x_1^{N_p} & x_2^{N_p} & x_3^{N_p} & \dots & x_D^{N_p} \end{bmatrix} \quad (1)$$

where, N_s represents the total count of rivers and a single sea:

$$N_s = \text{Number of rivers} + \underbrace{1}_{\text{sea}} \quad (2)$$

The remaining population $N_{streams}$ is given in Eq. (3):

$$N_{streams} = N_p - N_s \quad (3)$$

The quantity of water conveyed to a river or the sea is determined by the volume of water in flow. An estimation of the allocated streams for rivers and the sea is computed in the following manner:

$$NS_n = round\left\{\left|\frac{Cost_n - Cost_{N_s+1}}{\sum_{n=1}^{N_s} C_n}\right| \times N_{streams}\right\} \quad (4)$$

where, NS_n is the count of streams that contribute to individual rivers and the sea.

During the exploitation phase, the updated positions of variables are acquired using the following equations:

$$\vec{X}_{stream}(t+1) = \vec{X}_{stream}(t) + rand \times C \times \left(\vec{X}_{sea}(t) - \vec{X}_{stream}(t)\right) \quad (5)$$

$$\vec{X}_{stream}(t+1) = \vec{X}_{stream}(t) + rand \times C \times \left(\vec{X}_{river}(t) - \vec{X}_{stream}(t)\right) \quad (6)$$

$$\vec{X}_{river}(t+1) = \vec{X}_{river}(t) + rand \times C \times \left(\vec{X}_{sea}(t) - \vec{X}_{river}(t)\right) \quad (7)$$

Eqs. (5) and (6) are used for streams that merge into the sea and their respective rivers.

The iteration index is denoted by t. 1 < C < 2 denotes a constant, and rand signifies a random number uniformly distributed between 0 and 1. When a stream shows a lower cost function value than its associated river, their positions are interchanged. Similarly, in cases where a river exhibits a higher cost function value than the sea, the river and sea are interchanged.

The evaporation mechanism serves to prevent local optima and occurs when a river or stream is close to the sea, as determined by the following criterion:

$$\begin{cases} \text{if } \left\| \vec{X}^{t}_{sea} - \vec{X}^{t}_{river_j} \right\| < d_{max} \text{ or } rand < 0.1 \; j = 1, 2, 3, \ldots, N_{sr} - 1 \\ \text{perform raining process} \\ end \end{cases} \quad (8)$$

where, d_{max} is a small positive value that approaches zero over time and diminishes according to the specified formula:

$$d_{max^{i+1}} = d_{max^{i}} - \frac{d_{max^{i}}}{max\ iteration} \quad (9)$$

After fulfilling the evaporation process, the algorithm proceeds with the raining step. During this process, a new population of streams is generated at various locations. Calculation of the positions for the new streams is performed using the following formula:

$$X^{new}_{stream} = LB + rand \times (UB - LB) \quad (10)$$

In the context of LB (lower bound) and UB (upper bound), which define the optimization constraints, we can implement a mechanism for constrained problems to generate streams flowing directly to the sea. This approach enables a deeper exploration of the solution space in proximity to the sea, potentially leading to optimal solutions:

$$X^{new}_{stream} = X_{sea} + \sqrt{\mu} \times randn(1,\ D) \quad (11)$$

where, μ is a coefficient associated with proximity to the sea.

2.2.2 Moth flame optimization algorithm

Developed by Mirjalili [80], the Moth-Flame Optimization (MFO) algorithm is a nature-inspired metaheuristic method that replicates the navigation behavior of moths, using moonlight as a reference for orientation to solve optimization problems, as illustrated in Figure 3.

Figure 3. Conceptual model of the fly behavior of moths

The MFO algorithm treats candidate solutions as moths, using their positions in the search space to represent the problem variables. This enables the exploration of different dimensional spaces by adjusting the positional vectors of the moths. The algorithm employs a population-based approach, which represents moths as a matrix for efficient manipulation:

$$M = \begin{bmatrix} m_{1,1} & m_{1,2} & \cdots & \cdots & m_{1,d} \\ m_{2,1} & m_{2,2} & \cdots & \cdots & m_{2,d} \\ \vdots & \vdots & \vdots & \vdots & \vdots \\ m_{n,1} & m_{n,2} & \cdots & \cdots & m_{n,d} \end{bmatrix} \quad (12)$$

where, n represents the total moth population and d indicates the dimensionality of the problem space. The fitness value for each moth is stored in an array using the following representation:

$$OM = \begin{bmatrix} OM_1 \\ OM_2 \\ \vdots \\ OM_n \end{bmatrix} \quad (13)$$

Each moth's fitness value is computed by evaluating the fitness function using the moth's position vector (stored in the first row of matrix M). The resulting value from the fitness function is then allocated to the respective moth as its fitness score, such as OM1 in OM. In addition to moths, another important component of the algorithm is flames. A matrix akin to the one used for moths is employed to represent flames and is structured as follows:

$$F = \begin{bmatrix} F_{1,1} & F_{1,2} & \cdots & \cdots & F_{1,d} \\ F_{2,1} & F_{2,2} & \cdots & \cdots & F_{2,d} \\ \vdots & \vdots & \vdots & \vdots & \vdots \\ F_{n,1} & F_{n,2} & \cdots & \cdots & F_{n,d} \end{bmatrix} \quad (14)$$

where, n denotes the moth count and d represents the dimensionality. The matrices M and F share identical dimensions in Eq. (14). An array stores the fitness values of the flames, structured as:

$$OF = \begin{bmatrix} OF_1 \\ OF_2 \\ \vdots \\ OF_n \end{bmatrix} \quad (15)$$

The MFO algorithm employs a three-component system to find the global optimum in optimization problems, structured as:

$$MFO = (I, P, T) \quad (16)$$

where, I create a population of moths along with their corresponding fitness values:

$$I: \varnothing \rightarrow M, OM \quad (17)$$

In addition, the P function moves the moths:

$$P: M \rightarrow M \quad (18)$$

The function T returns a Boolean value: true when termination conditions are met, false otherwise:

$$T: M \rightarrow \{true, false\} \tag{19}$$

To update the moth position, we use the following equation:

$$M_i = S\left(M_i, F_j\right) \tag{20}$$

where, M_i, F_j indicates i-th moth and j-th flame, respectively, and S is the spiral function as follows:

$$S\left(M_i, F_j\right) = D_i.e^{bt}.\cos\left(2\pi t\right) + F_j \tag{21}$$

where, D_i is the distance between M_i and F_j, b is constant, t is randomly chosen in [−1, 1], and D_i is calculated using the following equation:

$$D_i = \left|F_j - M_i\right| \tag{22}$$

To enhance the exploitation phase, the number of flames is gradually decreased in relation to the number of iterations, following the equation shown below:

$$N_{flames} = round(N - I \times \frac{N-1}{T}) \tag{23}$$

During iteration I, N indicates the maximum flame count and T denotes the total iteration limit. The number of flames decreases as iterations progress.

2.2.3 Hybrid Water Cycle–Moth Flame Optimization algorithm

The WCAMFO hybrid algorithm aims to combine the strengths of the WCA and MFO algorithms, harnessing the benefits of each. While the WCA excels in the exploration phase, it lacks an efficient exploitation operator. On the other hand, the MFO algorithm, which emulates moths spiralling around artificial lights, demonstrates proficiency in exploiting the solution space. However, it is prone to occasionally becoming trapped in local optima [81].

In the WCAMFO algorithm, the foundational algorithm is the WCA. The initial enhancement in the WCA involves employing the spiral motion of moths to update the positions of streams and rivers. In the standard adjustment process of the WCA, the primary focus is on the region between the stream and the river. When determining the next position, the new position of the stream depends on how far it is from the river into which it flows [76]. Conversely, the MFO algorithm facilitates positional adjustments by moths freely in the vicinity of their associated flame. This flexibility enables the streams and rivers to use the spiral movement of moths to update their positions. By incorporating this capability, the hybrid WCAMFO algorithm significantly enhances its exploitation ability, leading to improved optimization performance [76].

Two processes are introduced in the WCAMFO algorithm to improve the randomization, first the raining process: This process is triggered when the gap between a river or stream and the sea drops below a predefined threshold value dmax. In the WCAMFO algorithm, the raining process is employed to generate new solutions. The other process is the random walk, which allows the random movement of streams within the solution space via a random walk, specifically using a Levy flight.

The WCAMFO algorithm allows streams to move to new positions using the following equation, which helps to make the algorithm more random [76]:

$$x_{i+1} = x_i + \text{Levy(dim)} \otimes x_i \tag{24}$$

where, x_{i+1} represents the next position, x_i denotes the immediate location, and dim indicates the number of decision variables in the problem space. Levy flight is determined through the application of the following formula:

$$\text{Levy(x)} = \frac{0.01 \times \sigma \times r_1}{|r_2|^{1/\beta}} \tag{25}$$

where, r_1 and r_2 are randomly generated numbers between 0 and 1, and σ is calculated as follows:

$$\sigma = \left(\frac{\Gamma\left(1+\beta\right) \times \sin\left(\frac{\pi\beta}{2}\right)}{\Gamma\left(\frac{1+\beta}{2}\right) \times \beta \times 2^{\left(\frac{\beta-1}{2}\right)}} \right)^{\frac{1}{\beta}} \tag{26}$$

2.3 Mathematical formulation of hybrid system components

2.3.1 Photovoltaic model

The impact of temperature on the PV generator's hourly output power P_{PV} is considered. The calculation of P_{PV} incorporates the PV generator's area A_{PV} (m^2) and the solar radiation on the tilted plane module G(t) (kW/m^2) using Eq. (27). Of note, the PV module's efficiency declines with rising temperature.

$$P_{PV} = \eta_{PV}.\eta_{inv}.A_{PV}.\gamma.\frac{G}{G_{STC}}\left[1+\gamma_T\left(T - T_{STC}\right)\right] \tag{27}$$

Solar PV module performance incorporates multiple efficiency factors: η_{PV} is the PV module efficiency, η_{inv} denotes the inverter efficiency; G_{STC} is the irradiance under standard test conditions (STC), which is 1 kW/m^2; T and T_{STC} indicate the PV cell's operating temperature and the temperature at STC (25 ℃), respectively. γ_T characterizes the module's maximum power variation per degree Celsius relative to the STC temperature of 25 ℃. For crystalline silicon, this coefficient typically ranges from -0.5 to -0.3%/℃ [82]. The derating factor γ accounts for the system performance losses, assumed to be 0.9 throughout this study [83]. The temperature at which a PV cell is operating can be estimated using a linear approximation using Eq. (28) [84].

$$T = T_a + \frac{G}{0.8}\left(T_{NOCT} - 20\right) \tag{28}$$

where, T (℃) is the PV cell operating temperature, T_a (℃) is the ambient air temperature, G(kW/m^2) is the incident solar irradiance on the PV module surface, and T_{NOCT} (℃) is the Nominal Operating Cell Temperature (typically between 45 and 48 ℃), which represents the cell temperature under

standard test conditions of 800 W/m² irradiance, 25 °C ambient temperature, and wind speed of 1 m/s. This formulation reflects the increase in cell temperature with increasing solar irradiance and ambient temperature.

2.3.2 Inverter

The hourly AC power output of the inverter is calculated as:

$$E_{inv,out}(t) = \eta_{inv}.E_{PV}(t) \tag{29}$$

where, $E_{\text{inv,out}}(t)$(W) is the inverter output power at hour t, $E_{PV}(t)$(W) is the DC power generated by the PV array at the same time, and η_{inv} denotes the inverter efficiency. This equation represents the conversion of DC power produced by the PV array into usable AC power, accounting for inverter losses.

2.3.3 Objective function

The NPC serves as the objective function in the optimization problem, which can be calculated as follows [85]:

$$NPC = cost - C_{ex} \times \frac{1}{CRF} \tag{30}$$

where, C_{ex} represents the net grid interaction cost, calculated as the difference between the energy purchased and the energy sold, the overall cost of the grid-connected system comprises the initial expense, replacement costs, and the ongoing operation and maintenance expenses for the components throughout the life span of the system, as given in Eq. (31) [85]:

$$\text{cost} = \sum_{k} \left[\left(C_{I,k} + C_{O,k} \times \frac{1}{CRF} + C_{R,k} \times R_k \right) \times P_k \right] \tag{31}$$

The component indicator k delineates cost elements where C_I, C_R, and C_O represent initial, replacement, and operational costs per kilowatt ($/kW), respectively. R_k indicates the single payment present worth, while CRF designates the capital recovery factor, both calculated through specified equations [18, 86]:

$$R_k = \sum_{n=1}^{N} \frac{1}{(1+j)^{L \times n}} \tag{32}$$

$$CRF = \frac{j(j+1)^{T_p}}{(j+1)^{T_p} - 1} \tag{33}$$

In this equation, j represents the real interest rate while N denotes the number of replacements for component k. L indicates the component's lifetime, and Tp represents the project duration (25 years), which aligns with the PV panels' expected lifespan. The real interest rate calculation employs Fisher's formula as follows [26]:

$$j = \frac{j' - f}{1 + f} \tag{34}$$

where, j represents the real interest rate, j' denotes the nominal interest rate, and f indicates the annual inflation rate.

2.3.4 Renewable fraction and zero-energy constraints

The RF represents the proportion of the total electrical energy supplied to the residential load that originates from renewable sources, namely PV generation in this study. It is calculated as the ratio between the annual PV energy production and the total annual energy supplied to the system, which includes both PV energy and energy purchased from the grid. An RF value close to unity indicates a high level of renewable penetration and reduced dependency on grid electricity. The calculation of the RF is determined as follows [87]:

$$E_{tot} = E_{PV} + E_{purch} \tag{35}$$

$$RF = \frac{E_{PV}}{E_{tot}} \tag{36}$$

where, E_{purch} represents the annual energy purchased from the grid (kWh/yr), E_{PV} is the annual PV energy (kWh/yr), and E_{tot} is the annual energy production (kWh/yr).

It should be noted that the RF is an annual, energy-based indicator and does not explicitly account for temporal mismatches between PV generation and load demand. In practical grid-connected applications, periods of surplus PV generation and grid electricity imports may still occur, even when high RF values are achieved. Consequently, while RF is a useful metric for evaluating the long-term contribution of renewable energy, it does not fully capture short-term operational constraints or grid interaction dynamics. For this reason, a zero-energy balance is introduced as a constraint to ensure that the overall annual energy consumption of the system is balanced by renewable energy generation. To achieve a ZEH, the total energy produced by the PV system must be equal to or greater than the household energy demand:

$$E_{PV} \geq E_{load} \tag{37}$$

where, E_{PV} refers to the total electrical energy output of the PV system and E_{load} is the amount of energy consumed by the house.

2.4 Electric vehicle charging characteristics

Several factors influence the process of EV charging, including the type of vehicle, battery technology, battery capacity, battery state of charge (SOC), charging power level, and charging behavior [88]. The following mathematical model simulates the typical charging profile of lithium-ion EV batteries [89]:

$$P(t) = \begin{cases} P_r & 0 < t \leq t_1 \\ P_r \dfrac{t_2 - t}{t_2 - t_1} & t_1 < t \leq t_2 \end{cases} \tag{38}$$

where, P(t) denotes the charging power at time t, P_r represents the rated charging power determined by the selected charging mode, and t_1, t_2 are the respective start and end times that define the variation in charging power as the battery nears full capacity.

This study only uses slow charging power (Mode 1) among the three charging classifications presented in Table 1 and Figure 4. The EV characteristics are summarized in Table 2.

Table 1. Parameters of the electric vehicle (EV) battery charging profile

	Mode 1	Mode 2	Modes 3 and 4
P_r (kW)	3.5	6.6	40
t_1 (h)	6.3	3.5	0.5
t_2 (h)	8	4	0.75

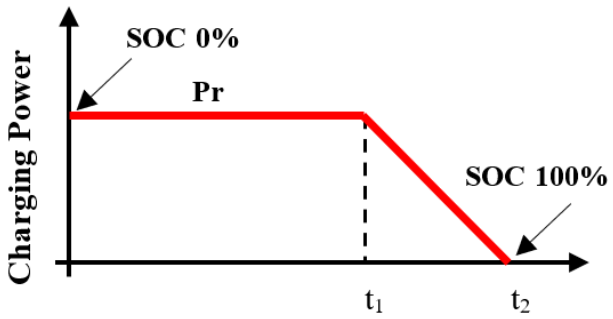

Figure 4. Charging profile of lithium-ion electric vehicle (EV) batteries [90]

Table 2. Characteristics of the electric vehicle (EV) chosen

Characteristics	Value
Battery capacity (kWh)	16
Autonomy (km)	80
Delay time (h)	4–8 h

2.5 Designed system specification

The technical and economic specifications are detailed in Table 3. The PV system features the CEM240P-60, a multi-crystalline module produced by the Algerian Manufacturer Condor. This module delivers 240 Wp with 14.7% efficiency at an upfront cost of 1312 $/kWp. DC to AC conversion is handled by an inverter operating at 95% efficiency, requiring an initial investment of 600 $/kW and replacement cost of 300 $/kW, with a ten-year service life.

Table 3. Technical characteristics and cost-related attributes of the system

Inputs	Value
Project lifetime (yr)	25
PV module lifetime (yr)	25
Inverter lifetime (yr)	10
Inverter efficiency (%)	95
Nominal discount rate (%)	8
Real interest rate (%)	4
PV module cost ($/kWp)	1312
Inverter cost ($/kW)	600
Grid sell-back price ($/kWh)	0.148

Sonelgaz, Algeria's national utility company, manages the power grid, while the Regulatory Commission for Electricity and Gas oversees electricity pricing. Residential customers typically use the 54 M tariff rate. Table 4 provides comprehensive details about Algeria's residential feed-in tariff structure, which consists of four pricing tiers, the first tier applies to consumption between 0 and 125 kWh at a rate of 1.778 DZD/kWh, the second tier covers consumption between 126 and 250 kWh at a rate of 4.178 DZD/kWh, the third tier applies to consumption between 251 and 1000 kWh at a rate of 4.182 DZD/kWh, and the fourth tier applies to consumption exceeding 1,000 kWh at a rate of 5.479 DZD/kWh.

Table 4. Residential feed-in tariff rate

Bands	Energy Cost	
	(cDA/kW)	($/kWh)
Band 1	1.778	0.013
Band 2	4.178	0.031
Band 3	4.812	0.035
Band 4	5.479	0.044

3. CASE STUDY

This section provides details about the site's location, load profile, meteorological conditions, as well as the technical and economic input data used in modeling the hybrid PV grid system.

3.1 Site description

This case study focuses on a low-energy pilot house built under the European MED-ENEC initiative, as part of a scientific partnership between Algerian Renewable Energy Centre (CDER) and the National Center for the Study and Integrated Research of Buildings (CNERIB). The dwelling is located in the suburban region of Algiers, within the Souidania Municipality. With an approximate area of 90 m^2, the house is designed to accommodate a family of five. It comprises three rooms, a kitchen, toilet, bathroom, courtyard, and corridor. Figure 5 provides a general overview of house [73].

Figure 5. General view of the house (Souidania, Algiers)

3.2 Meteorological characteristics

The solar resources utilized in this research were sourced from the NASA Surface Meteorology and Solar Energy (SSE) database. The dataset includes information on global horizontal solar radiation, which varies between 2.23 and 7.26 kWh/m^2/day.

The location receives an estimated average annual solar radiation of 4.85 kWh/m^2/day, accompanied by a clearness index of 0.58, as depicted in Figure 6. The selected location offers favorable conditions for the implementation of PV systems, as it receives sufficient solar radiation for efficient energy generation.

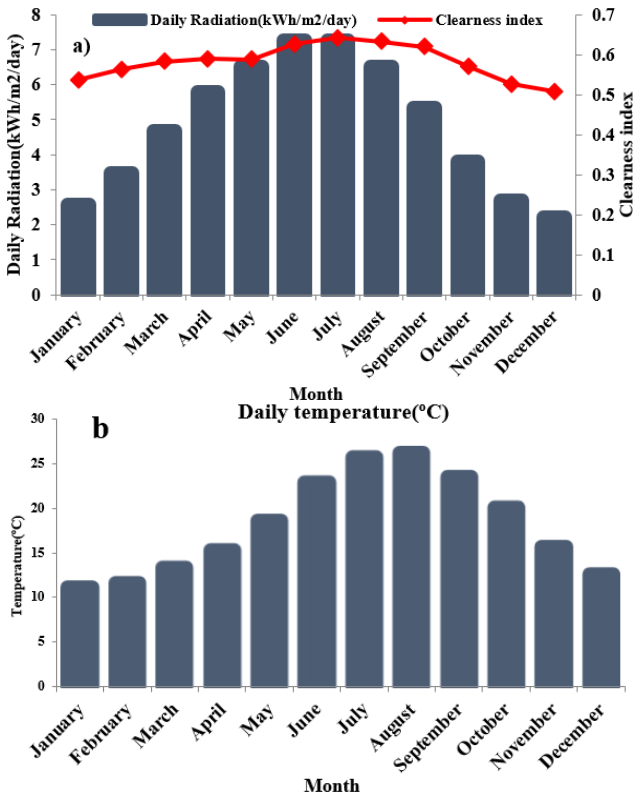

Figure 6. Meteorological characteristics of the site: a) solar radiation data and b) ambient temperature

3.3 Load profile

Initially, we conducted an evaluation of electricity consumption by considering the use of efficient electrical equipment, excluding EVs. Table 5 summarizes the electrical equipment used in the house, along with its corresponding characteristics.

Table 5. Characteristics of electrical equipment

Area	Device	Power (W)	Quantity
Living room	L1: Light	11	3
	E1: TV	160	1
	E2: Demo SAT	30	1
Room 1	L2: Light	11	2
	Fan	75	2
Room 2	L3: Light	11	2
	Laptop	90	1
	Wi-Fi	60	1
	Mobile charger	15	1
Room 3	L4: Light	11	2
	Tablet	30	1
Kitchen	L5: Light G	15	1
	E3: Refrigerator	40	1
Bathroom	L6: Light	11	1
	E4: Washing machine	1250	1
WC	L7: Light	11	1
Corridor	L8: Light	6	2

In this part, two hourly domestic load patterns are considered for the house: summer profile (from April to September) and winter profile (from October to March). The daily average consumption is 5.2 kWh/day. Figure 7 shows the basic load profile without the EV. Electricity consumption is typically higher during summer months compared to winter due to the increased use of ventilation requirements and additional lighting.

As EVs are still in the early planning stages in Algeria, adequate data concerning their actual charging operations is scarce. Therefore, to study the impact of adding an EV to the basic domestic electrical load, the electrical consumption of an EV is added to the daily load profile.

According to Moon et al. [91], over 85% of EV charging occurs at home, with owners typically charging their vehicles overnight. Consequently, we chose to initiate the charging process for the EV battery at nighttime, specifically from 01:00 to 05:00. A duration of more than 4 h achieves at least an 80% EV charge. Figure 8 provides a visual representation of both daily load profiles, considering the inclusion of the EV. In winter and summer, peak consumption occurs between 01:00 and 05:00, which corresponds to the charging period of the EV. Additionally, from 14:00 to 17:00 and 20:00 to 23:00, the summer season often sees elevated electricity demand relative to winter, primarily driven by cooling loads associated with high ambient temperatures.

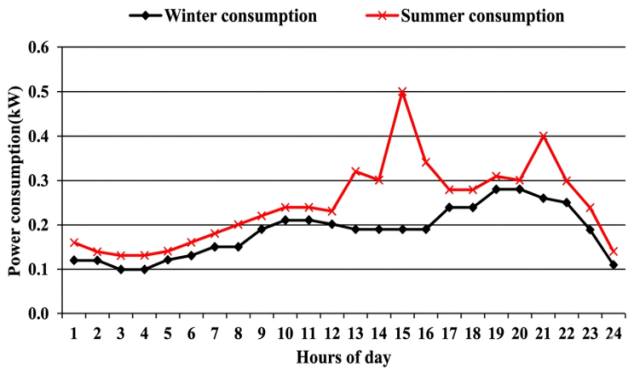

Figure 7. Daily load consumption

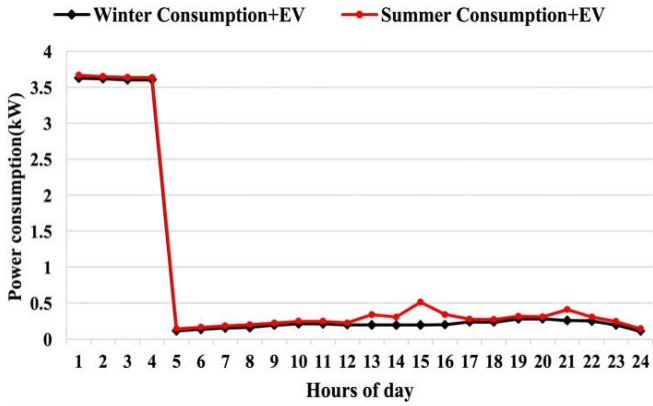

Figure 8. Daily load consumption with the electric vehicle (EV)

4. RESULTS AND DISCUSSION

The modeling and optimization of the system in this study were carried out using MATLAB software. The code was developed to incorporate the WCAMFO hybrid algorithm, which is employed to identify the optimal configuration of a grid-connected PV system under two distinct scenarios.

Scenario 1: The grid-connected PV system is configured such that all the produced PV energy is sold to the grid, while

all the energy consumed by the household is purchased from the grid. In other words, any energy generated by the PV system is fed back into the grid, and households rely entirely on the grid for their energy needs. Eq. (39) shows the hourly profile of PV energy transactions with the grid, encompassing both energy purchases and injections.

$$E_{purch}(t) = E_{load}(t) \ and \ \ E_{sold}(t) = E_{PV}(t) \tag{39}$$

Scenario 2: The home purchases only the electricity needed from the grid. Any surplus energy generated by the PV system is fed into the grid and sold to the electricity provider. This setup allows the home to offset its electricity consumption by using PV-generated electricity and potentially earn credits or financial compensation for the excess energy supplied to the grid.

$$\begin{cases} E_{purch}(t) \\ = E_{load}(t) - E_{PV}(t), E_{sold}(t) = 0, \text{if } E_{load}(t) > E_{PV}(t) \\ E_{sold}(t) \\ = E_{PV}(t) - E_{load}(t), \ E_{purch}(t) = 0, \text{if } E_{load}(t) < E_{PV}(t) \end{cases} \tag{40}$$

Both energy scenarios' optimization problems are formulated using Eq. (41):

$$\text{Min}\{NPC(x)\} x \in ss \quad x = (P_{PV})$$
$$\text{Subject to} \begin{cases} S \leq 16\ m^2 \\ RF \geq 30\% \\ E_{PV} \geq E_{Load} \end{cases} \tag{41}$$

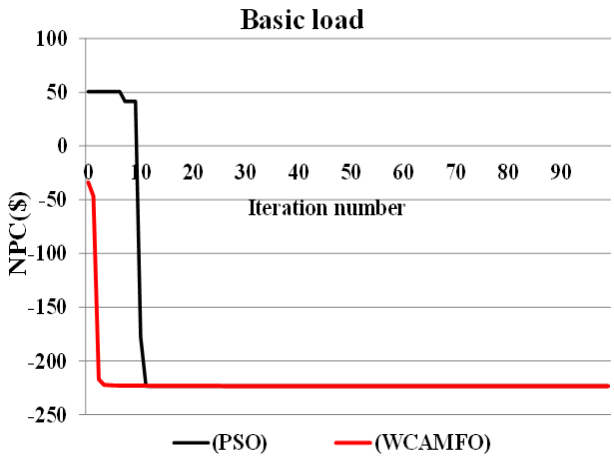

Figure 9. Net present cost (NPC) convergence comparison between Water Cycle–Moth Flame Optimization (WCAMFO) and particle swarm optimization algorithm (PSO) for basic load

NPC serves as the objective function. The constraints include the RF, available roof area, and zero energy consumption requirements. The analysis evaluates the hybrid grid-PV system over a 25-year lifecycle to assess its technical, economic, and environmental performance under two different energy scenarios. These scenarios are constructed based on previously established input parameters. The population size is set to 50, with the algorithm executed over 100 iterations. First, the WCAMFO algorithm is compared with PSO. Figure 9 presents the convergence behavior of both algorithms in minimizing the NPC under the basic load scenario. WCAMFO converges to the optimal NPC value of −223.269 $ within fewer than five iterations and exhibits stable convergence without oscillatory behavior. In contrast, PSO requires approximately 10–12 iterations to reach a comparable solution. These results demonstrate the faster convergence rate of WCAMFO. The improved performance of WCAMFO is attributed to its hybrid search mechanism, which provides an effective balance between global exploration and local exploitation. Conversely, PSO is more susceptible to premature convergence and oscillations due to its velocity update formulation and sensitivity to parameter settings. Consequently, WCAMFO achieves reduced computational effort and improved stability, making it suitable for complex nonlinear optimization problems such as energy management systems with EV integration.

Figures 10 and 11 illustrate the convergence curves for the different load profile scenarios. WCAMFO achieves the optimal solution within three iterations for both scenarios. However, the first scenario achieves a superior minimum value (NPC), whereas the second energy scenario yields a higher RF.

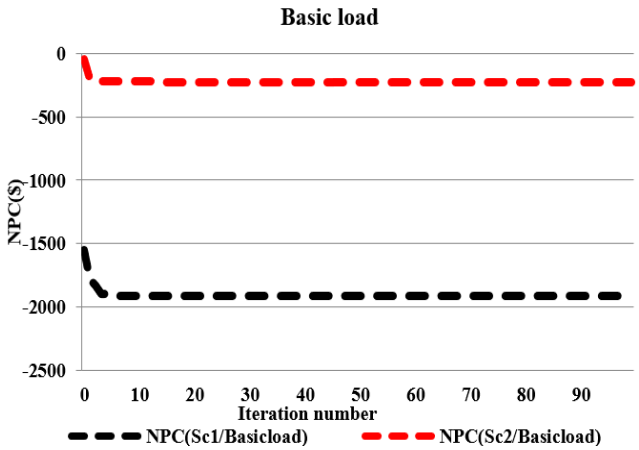

Figure 10. Net present cost (NPC) convergence curve for basic load using the Water Cycle–Moth Flame Optimization (WCAMFO) algorithm

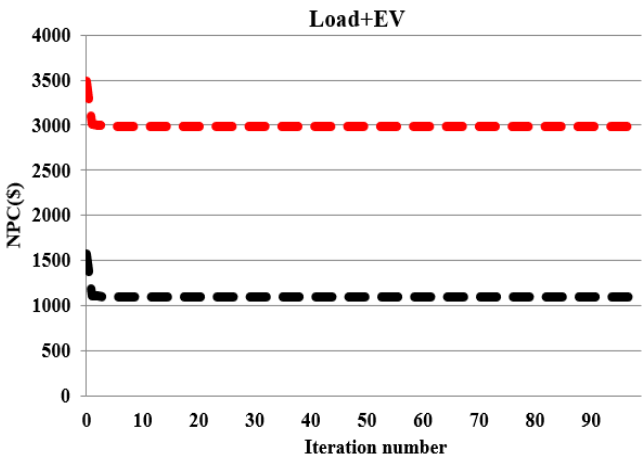

Figure 11. Net present cost (NPC) convergence curve for load & electric vehicle (EV) using the Water Cycle–Moth Flame Optimization (WCAMFO) algorithm

Initially, the system is simulated using the basic load profile for both energy scenarios to identify the optimal solution that meets the criteria of an RF exceeding 30%, a roof area of less than 16 m^2, and zero energy. Subsequently, the simulation was repeated for the load profile incorporating the integrated EV,

employing identical configurations, and the outcomes were compared and analyzed.

Beyond the convergence performance, the obtained optimization results provide important insights into the practical integration of PV systems in residential buildings in Algeria. The rapid convergence of the WCAMFO algorithm within a few iterations indicates its suitability for real-world applications where computational efficiency is essential for system sizing and economic assessment. The lower NPC observed under the basic load scenario reflects the reduced system stress and more stable demand pattern, whereas the load + EV scenario introduces higher energy demand and variability, resulting in increased NPC despite improved RF.

Furthermore, for the purpose of validating the outcomes generated through the WCAMFO algorithm, a comparative analysis was conducted with the HOMER software. The comparison focused on key metrics such as NPC, COE, and RF. The results are summarized in Tables 6 and 7.

Table 6. Simulation results for the basic load

	Basic Load		
	WCAMFO (Sc1)	**WCAMFO (Sc2)**	**HOMER (Sc2)**
NPC ($)	-1941.88	-223.4	31.44
COE ($/kWh)	-0.023	-0.0032	0.00049
PV production (kWh/year)	3693.7	3693.7	3471
Grid Purchases (kWh/year)	1658.31	779.73	759
Grid Sales (kWh/year)	3693.7	2815.11	2481
RF (%)	69	82.6	81.3

Note: NPC = net present cost; COE = cost of electricity; PV = photovoltaic; RF = renewable fraction; WCAMFO = Water Cycle–Moth Flame Optimization; Sc1 = scenario1; Sc2 = scenario2; HOMER = Hybrid Optimization Model for Electric Renewables

Table 7. Simulation results for Load + EV

	Load + EV		
	WCAMFO (Sc1)	**WCAMFO (Sc2)**	**HOMER (Sc2)**
NPC ($)	1093.85	2988.76	3048
COE ($/kWh)	0.0063	0.019	0.0203
PV production (kWh/year)	3693.7	3693.7	3631
Grid Purchases (kWh/year)	7356.48	6326.03	6331
Grid Sales (kWh/year)	3693.7	2663.24	2481
RF (%)	33.4	36.86	36.5

Note: NPC = net present cost; COE = cost of electricity; PV = photovoltaic; RF = renewable fraction; WCAMFO = Water Cycle–Moth Flame Optimization; HOMER = Hybrid Optimization Model for Electric Renewables

For the basic load, the optimal solution consists of a 2.28 kWp PV system and a 2.5 kW converter. In y scenario 1, the COE for the system is -0.023 $/kWh, while in Energy scenario 2, it is -0.0032 $/kWh. The NPC is -1941.88$ for scenario 1 and -223.4$.

For scenario 2. The optimal system demonstrates significant performance, achieving a RF of 69% in scenario 1 and 82.6% in scenario 2. Furthermore, both energy scenarios result in an annual surplus of electricity sold to the grid, with 3693.7 kWh/year for Energy scenario 1 and 2815.11 kWh/year for Energy scenario 2, surpassing the energy purchased from the grid, which amounts to 1658.31 kWh/year for scenario 1 and 779.73 kWh/year for scenario 2.

Upon connecting the EV, the energy obtained from the grid increases significantly, reaching 7356.48 kWh/year for scenario 1 (compared to the initial 1658.31 kWh/year) and 6326.03 kWh/year for scenario 2 (compared to the initial 779.73 kWh/year). This increase in grid energy consumption directly correlates with a notable decrease in the RF, dropping from 69% to 33.4% for scenario 1 and 82.6% to 36.8% for scenario 2. Consequently, the expenses related to grid purchases also escalate, rising from 44.88$/year to 237.06$/year for scenario 1 and from 20.95$/year to 203.79$/year for scenario 2.

Moreover, the NPC of the system increased from -1941.88 $ (basic load) to 1093.8$ (load + EV) for scenario 1 and from -223.4$ (basic load) to 2988.76$ (load + EV) for scenario 2, which can be attributed to the heightened grid purchases. Despite this, the PV system successfully met the energy requirements of the load + EV in both energy scenarios and generated a total income of 316.99$ and 195.7$, respectively. The HOMER simulations closely aligned with our WCAMFO outcomes, thus validating the reliability of our optimization approach. For the Basic Load, WCAMFO algorithm outperformed HOMER in economic terms, showing negative NPC values. WCAMFO showed an NPC of -223.4$, compared to HOMER's positive 31.44$, reflecting substantial economic benefits. The COE was also negative in WCAMFO energy scenarios, implying earnings from energy produced. Additionally, the RF was higher in WCAMFO (82.6%) than in HOMER (81.3%). For Load + EV, both algorithms indicated increased costs. WCAMFO scenario 1 had a positive NPC (1093.85$), and scenario 2 showed even higher costs (2988.76$), similar to HOMER (3048$). Despite this, WCAMFO demonstrated lower COE values, indicating more cost-effective solutions. RF values were lower due to the additional load from the EV, but WCAMFO still showed slightly better economic performance compared to HOMER.

The results unequivocally demonstrate that the WCAMFO algorithm performs comparably to HOMER, with slight variations in the results. This validation establishes the reliability and accuracy of the WCAMFO algorithm and further validates its versatility. Figures 12 and 13 present the hourly energy balance simulations for the basic load in scenarios 1 and 2, respectively.

Figures 14 and 15 display the hourly energy balance simulations for the load + EV in both energy scenarios. Figures 12(a)-15(a) for Energy scenarios 1 and 2 show that during winter days, the available PV power is insufficient for fulfilling the energy needs of the household. Conversely, Figures 12(b) and 13(b) demonstrate that on summer days, the energy generated by the PV system exceeds the load in both energy scenarios. This indicates that the PV system adequately fulfills the load demand. In scenario 1, excess power is purchased from the grid, and PV energy is sold back to the grid. In Energy scenario 2, surplus energy is consumed internally, and any remaining surplus is injected into the grid. Furthermore, Figures 14(b) and 15(b) illustrate that from 07:00 to 22:00, the PV-generated energy surpasses the load demand. Nevertheless, between midnight and 06:00, the load experiences an increase caused by the charging of EV batteries, predominantly occurring during the nighttime from 01:00 to 06:00.

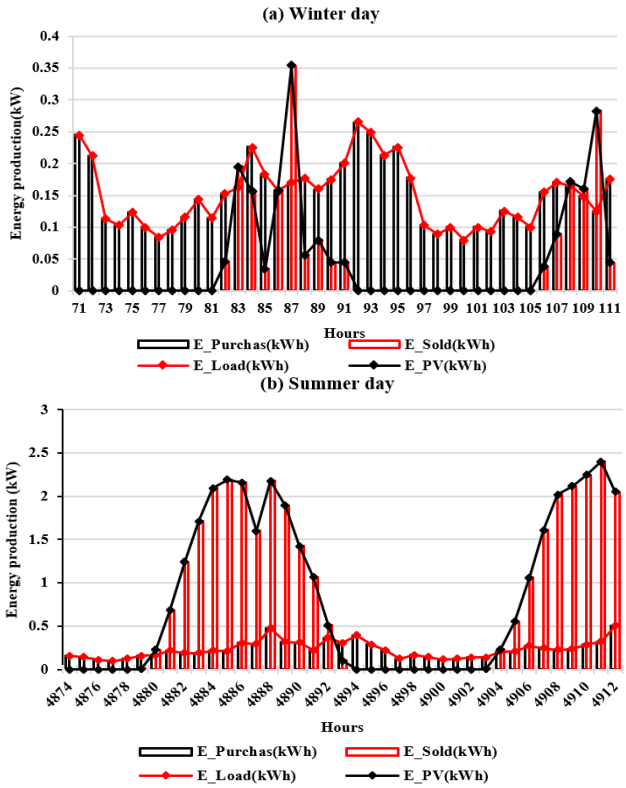

Figure 12. Hourly energy balance for the basic load (Scenario 1): (a) winter day and (b) summer day

Note: E_Purchas= energy purchased from the grid; E_Sold= energy is sold to the grid; E_Load= energy of load; E_PV= energy production of PV

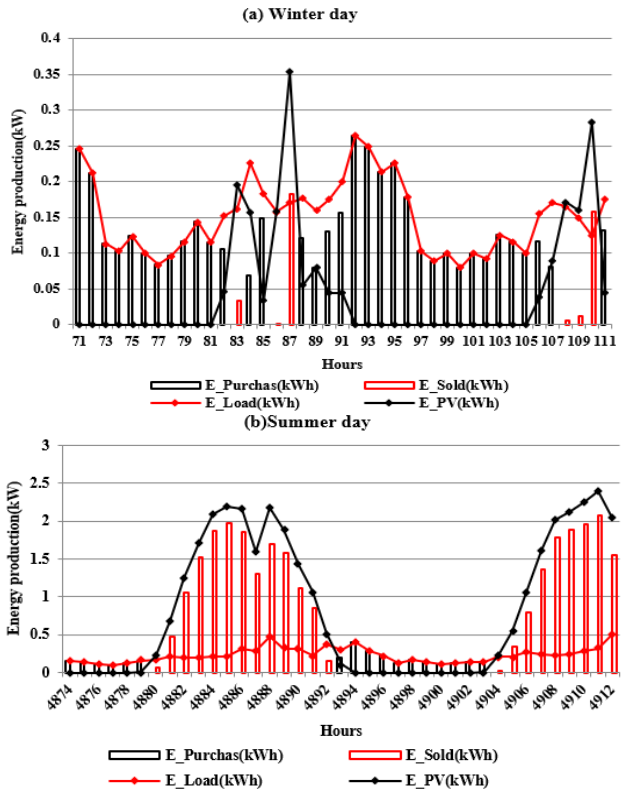

Figure 13. Hourly energy balance for the basic load (Scenario 2): (a) winter day and (b) summer day

4.1 Monthly variation analysis of energy generation in the designed system

Figure 16 shows that the monthly purchased energy from the grid is consistently lower than the energy sold to the grid in the basic load case. This leads to positive energy balances annually for all months.

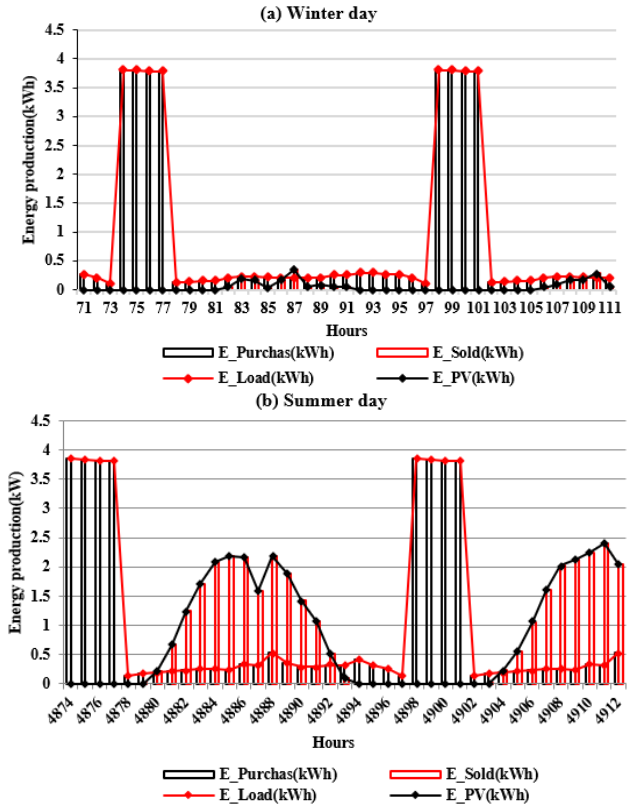

Figure 14. Hourly energy balance for load + EV (scenario 1): (a) winter day and (b) summer day

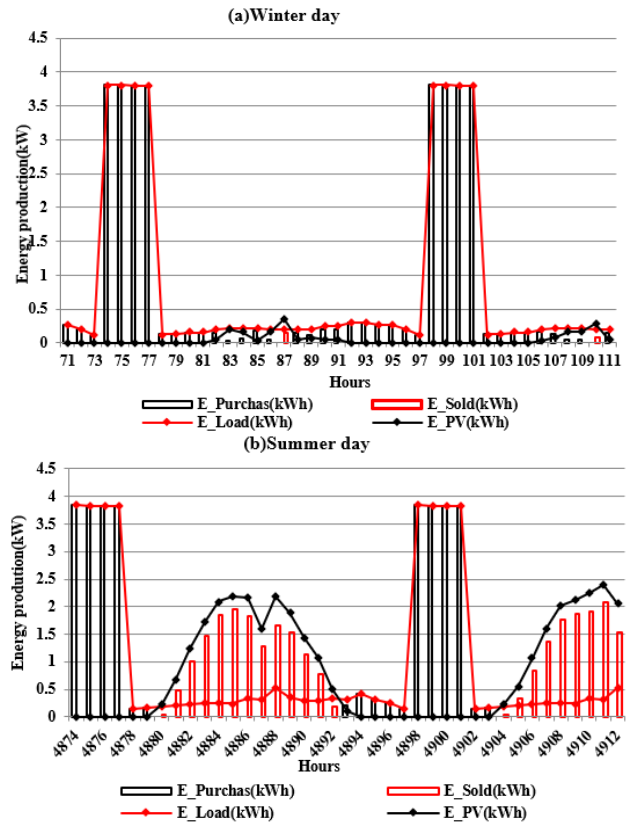

Figure 15. Hourly energy balance for load+EV (scenario 2): (a) winter day and (b) summer day

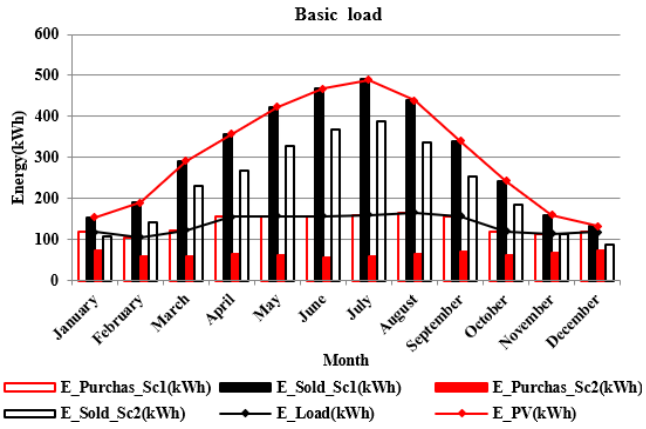

Figure 16. Average monthly energy output of the designed system for the basic load (scenario 1, scenario 2)

Conversely, Figure 17 illustrates that in both load + EV energy scenarios, monthly grid electricity purchases exceed the amount of energy exported back to the grid. This outcome leads to negative energy balances throughout the months, indicating an overall energy deficit.

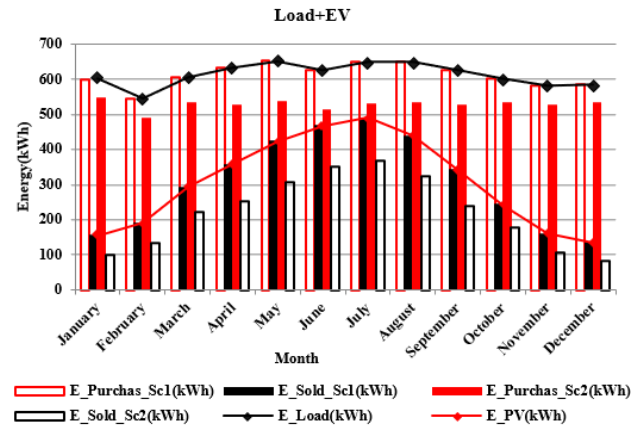

Figure 17. Average monthly energy output of the designed system for the load + EV (scenario 1, scenario 2)

4.2 Average monthly net grid interaction cost

Figures 18 and 19 show the variation of the net grid interaction cost (C_{ex}), which is found to be more favorable in scenario 1 than in scenario 2 for both profiles. In the basic load profile, C_{ex} shows an increasing trend during the summer months, peaking in July at 70.57 $/month for scenario 1 and 57.2 $/month for scenario 2.

Conversely, a decline is observed throughout the winter, culminating in a minimum level in December at 16.04 $/month for scenario 1 and 10.77 $/month for scenario 2. For the load + EV case, C_{ex} follows a similar trend, rising during the summer months, reaching its maximum value in July (54.25 $/month for scenario 1 and 39.67 $/month for scenario 2), and decreasing during winter, culminating in a minimum in the month of December (0.21 $/month for scenario 1 and −5.86 $/month for scenario 2). Overall, these findings underscore the advantageous impact on the system's profitability, especially during the summer season.

4.3 Monthly variation of the carbon mitigation factor CO_2

Based on estimated carbon emissions from the grid in Algeria, which amount to 517 g/kWh [85], Figures 20 and 21 show the monthly variation of the carbon mitigation for the basic load and load + EV, respectively. The mitigation of CO_2 emissions is considerably greater during the summer months than during winter in both considered energy scenarios. Furthermore, Energy scenario 1 demonstrates a higher level of CO_2 gas attenuation for both load profiles. In fact, it reached 86.22 kg in August for the basic load profile and 335.48 kg for the load + EV profile.

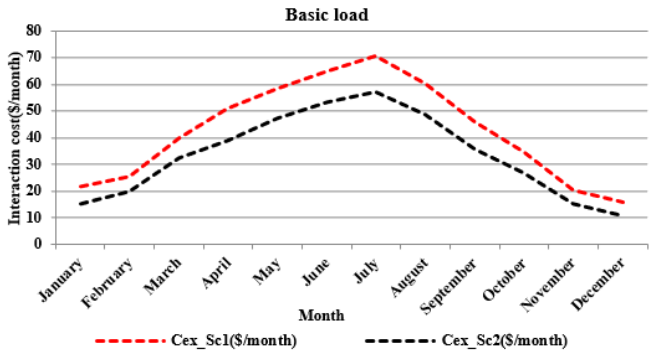

Figure 18. Average monthly net grid interaction cost (C_{ex}) for the basic load (scenario 1, scenario 2)

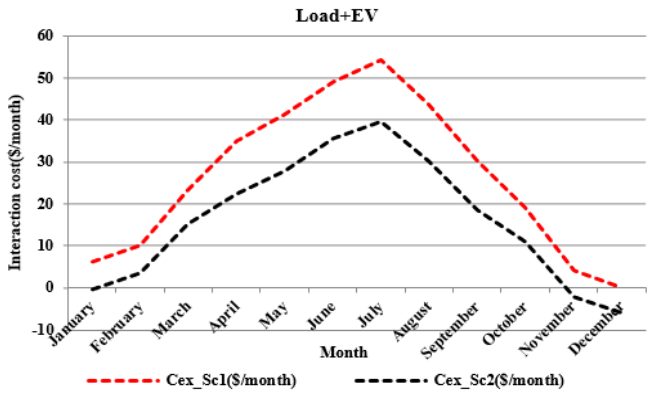

Figure 19. Average monthly net grid interaction cost C_{ex} for the load + EV (scenario 1, scenario 2)

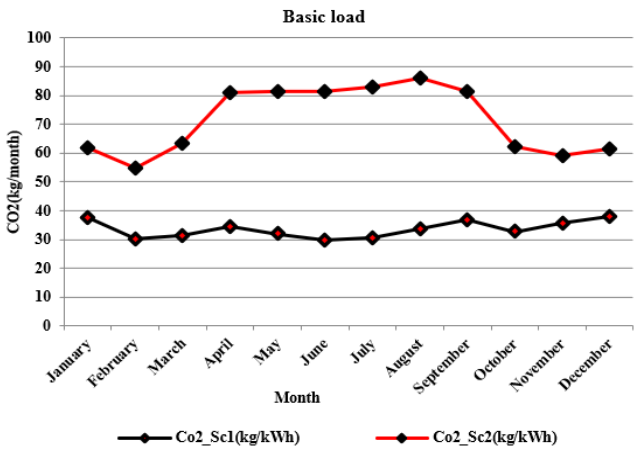

Figure 20. Monthly variation of the carbon mitigation factor CO_2 for the basic load in the two energy scenarios

4.4 Impact of RF on net present cost, cost of electricity, photovoltaic production, and grid sales profiles

Figures 22 and 23 illustrate the strong impact of the RF on

various parameters, including NPC, COE, PV production, and grid sales, for the (load + EV) profile.

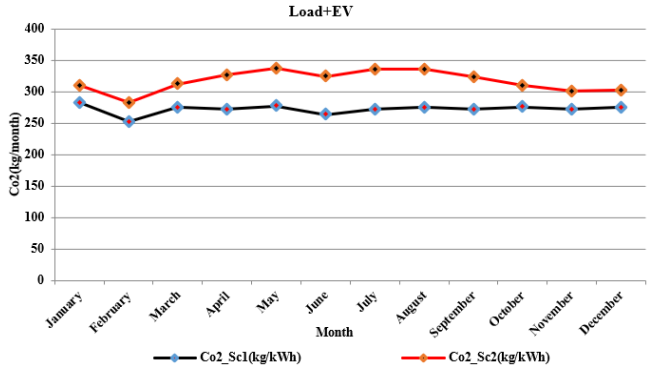

Figure 21. Monthly variation of the carbon mitigation factor CO_2 for (load + EV) in both energy scenarios

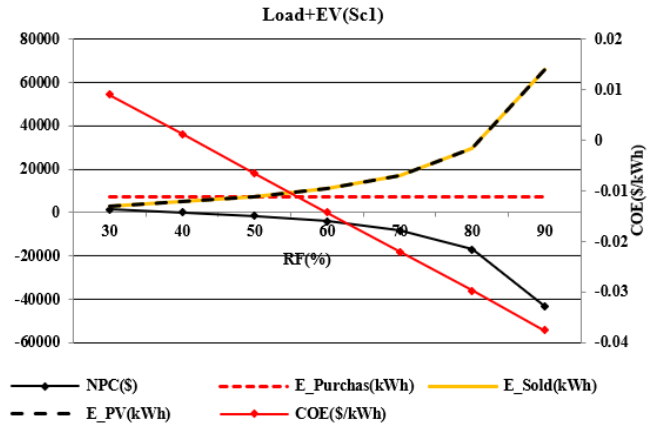

Figure 22. Effect of renewable fraction (RF) on net present cost (NPC), cost of electricity (COE), photovoltaic (PV) production, and grid sales (load + EV in scenario 1)

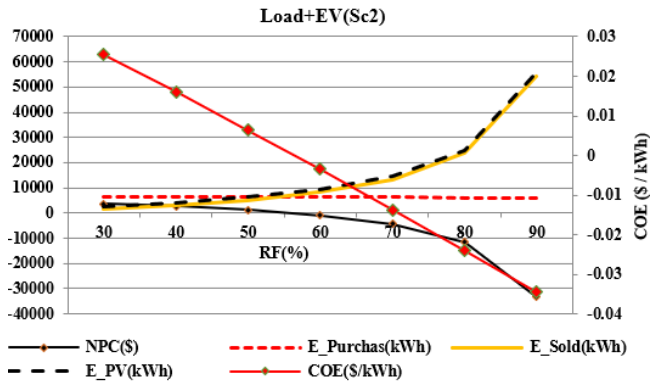

Figure 23. Effect of renewable fraction (RF) on net present cost (NPC), cost of electricity (COE), photovoltaic (PV) production, grid sales, and grid purchases (load + EV in scenario 2)

The COE experiences a decline, reducing from 0.009 $/kWh to -0.0375 $/kWh in energy scenario 1and from 0.0254 $/kWh to -0.346 $/kWh in scenario 2, as the RF increases from 40% to 90%. The NPC exhibits a similar trend, decreasing from 1475.99 $ to -43,071.5 $ in scenario 1 and from 3601.82 $ to -33,394.6 $ in scenario 2, with an increase in RF from 30% to 90%. Moreover, PV production and grid sales demonstrate an upward trend in both energy scenarios as the RF increases from 30% to 90%. In scenario 1, PV production and grid sales rise from 3152.6 to 66,207.93 kWh/yr. Similarly, in scenario 2, PV production increases from 2727.34 to 55,583.2 kWh/year, whereas grid sales increase from 1734.67 to 54,403.2 kWh/year.

4.5 Effect of photovoltaic-rated power on net present cost and grid sales

Figures 24 and 25 showcase the significant impact of PV rated capacity on NPC, grid sales and purchases, and roof space for the load + EV profile. In scenario 1, the NPC decreases from 1475.99$ to -43,071.5$ when the PV-rated capacity increases from 2 to 41 kWp. Similarly, in Energy scenario 2, the NPC decreases from 3601.82$ to -33,394.6$ with the same increase in PV-rated capacity.

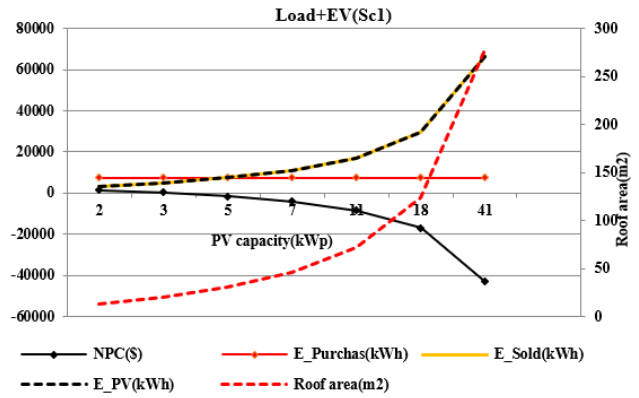

Figure 24. Effect of photovoltaic (PV)-rated power on net present cost (NPC) and grid sales (load + EV in scenario 1)

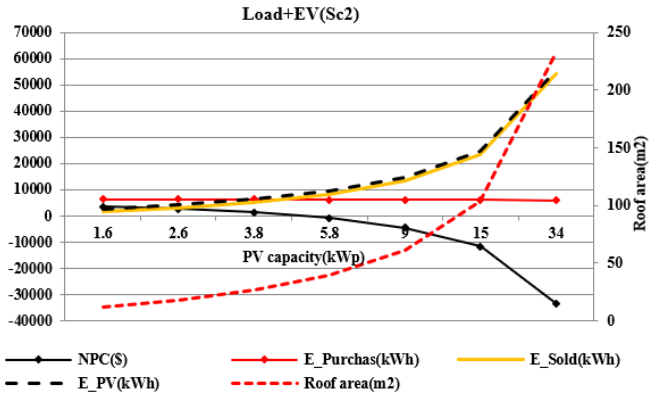

Figure 25. Effect of photovoltaic (PV)-rated power on net present cost (NPC), and grid sales (load + EV in scenario 2)

Consequently, the increase in PV-rated capacity leads to a substantial increase in the quantity of surplus energy exported to the grid in both energy scenarios. For scenario 1, grid sales increase from 3152.6 to 66,207.93 kWh/year with grid purchases of 7356.48 kWh. In scenario 2, grid sales increase from 1734.67 to 54,403.2 kWh/year, which leads to a decrease in grid purchases from 6363.81 to 6176.02 kWh/year. A notable positive correlation exists between PV capacity and the amount of roof space needed. This relationship emphasizes the importance of considering available space when decisive optimal PV capacity for a given installation.

From a practical perspective, these findings are particularly relevant to Algerian residential buildings, where the deployment of PV systems is often constrained by limited roof

area, variability in household electricity consumption, and economic considerations. In northern coastal regions, characterized by moderate solar irradiance, the optimization results indicate that cost-effective PV integration requires careful system sizing and effective load management strategies. Conversely, in the high plateau and southern regions, higher solar irradiance levels substantially enhance PV energy production, leading to reduced grid dependency and lower NPC under comparable system configurations.

In this context, although the proposed WCAMFO-based optimization framework is validated through comparison with HOMER, its generalization capability is further supported by its evaluation under multiple load profile scenarios, including EV integration and different seasonal operating conditions. These scenarios represent a wide range of realistic operating environments and demonstrate the robustness of the algorithm in responding to variations in energy demand and solar resource availability. Furthermore, the framework is data-driven and parameterized, which facilitates its adaptation to other geographical regions by incorporating region-specific solar irradiance, temperature, and load characteristics.

5. CONCLUSION

This study evaluates the feasibility of a ZEH in northern Algeria, integrating a grid-connected PV system and an EV. The WCAMFO algorithm was used to optimize the system, considering NPC as the primary variable, and RF, roof area, and zero energy as constraints. A detailed sensitivity analysis was conducted to assess system performance under different scenarios. The WCAMFO algorithm was compared to HOMER software for hybrid system optimization, revealing superior outcomes in both load profiles. The findings reveal that for the basic residential load, the optimal configuration includes a 2.28 kWp PV system and a 2.5 kW converter. The system achieves a COE of -0.023 $/kWh in scenario 1 and -0.0032 $/kWh in scenario 2, with NPC values of -1941.88$ and -223.4$, respectively. Renewable energy contribution reached an RF of 69% in scenario 1 and 82.6% in scenario 2, highlighting the system's economic and environmental benefits. However, integrating an EV significantly increases energy demand, reducing the RF to 33.4% in scenario 1 and 36.86% in scenario 2 due to higher grid reliance. To tackle this challenge, the system was reconfigured to an optimized setup comprising a 4.54 kWp PV system and a 5 kW converter. This adjustment ensured that grid energy exports matched or surpassed imports, resulting in enhanced performance metrics, including improved COE, increased PV energy production, and a more favorable energy balance.

These results highlight the importance of scaling up renewable energy utilization and adopting advanced energy management strategies to effectively integrate EVs into residential energy systems. Future research should focus on enhancing the proposed WCAMFO algorithm through adaptive parameter tuning, multi-objective optimization, and uncertainty modeling related to solar irradiance, electricity tariffs, and EV charging behavior. In addition, the integration of intelligent energy management strategies such as demand-side management, coordinated EV charging, and vehicle-to-home or vehicle-to-grid functionalities could significantly reduce grid dependency and improve system flexibility. Extending the proposed framework to include energy storage systems and validating it across different climatic regions and residential building types would further support the scalable and sustainable deployment of ZEHs with integrated EVs.

ACKNOWLEDGMENT

The authors extend their prayers to the late Professor Abdel-Rahman Hamidat, their cherished mentor, who regrettably succumbed to Covid-19 on August 16, 2021. They beseech God's grace, forgiveness, and blessings to encompass him.

REFERENCES

[1] Mohammed, T., Al-Amin, A.Q. (2018). Climate change and water resources in Algeria: Vulnerability, impact and adaptation strategy. Economic and Environmental Studies, 18(1): 411-429. https://doi.org/10.25167/ees.2018.45.23

[2] Friedlingstein, P., O'sullivan, M., Jones, M.W., Andrew, R.M., et al. (2020). Global carbon budget 2020. Earth System Science Data, 12(4): 3269-3340. https://doi.org/10.5194/essd-12-3269-2020

[3] Bouznit, M., Pablo-Romero, M.D.P., Sánchez-Braza, A. (2020). Measures to promote renewable energy for electricity generation in Algeria. Sustainability, 12(4): 1468. https://doi.org/10.3390/su12041468

[4] UNFCCC. (2015). Nigeria's Intended Nationally Determined Contribution.

[5] Díaz-Cuevas, P., Haddad, B., Fernandez-Nunez, M. (2021). Energy for the future: Planning and mapping renewable energy. The case of Algeria. Sustainable Energy Technologies and Assessments, 47: 101445. https://doi.org/10.1016/j.seta.2021.101445

[6] Zahraoui, Y., Khan, M.R.B., AlHamrouni, I., Mekhilef, S., Ahmed, M. (2021). Current status, scenario, and prospective of renewable energy in Algeria: A review. Energies, 14(9): 2354. https://doi.org/10.3390/en14092354

[7] Ministry of Energy and Mines (2020). National Energy Balance 2019. Algiers, Algeria.

[8] Vimpari, J., Junnila, S. (2019). Estimating the diffusion of rooftop PVs: A real estate economics perspective. Energy, 172: 1087-1097. https://doi.org/10.1016/j.energy.2019.02.049

[9] Mokhtara, C., Negrou, B., Settou, N., Gouareh, A., Settou, B. (2019). Pathways to plus-energy buildings in Algeria: Design optimization method based on GIS and multi-criteria decision-making. Energy Procedia, 162: 171-180. https://doi.org/10.1016/j.egypro.2019.04.019

[10] Semache, A., Hamidat, A., Benchatti, A. (2015). Impact study of the solar energy on the energy performances of the rural housing in Algeria. International Journal of Heat and Technology, 33(4): 229-236. http://doi.org/10.18280/ijht.330431

[11] Aziz, A.S., Tajuddin, M.F.N., Adzman, M.R., Mohammed, M.F., Ramli, M.A. (2020). Feasibility analysis of grid-connected and islanded operation of a solar PV microgrid system: A case study of Iraq. Energy, 191: 116591. https://doi.org/10.1016/j.energy.2019.116591

[12] Cui, Y., Zhu, J., Meng, F., Zoras, S., McKechnie, J., Chu, J. (2020). Energy assessment and economic sensitivity

analysis of a grid-connected photovoltaic system. Renewable Energy, 150: 101-115. https://doi.org/10.1016/j.renene.2019.12.127

[13] Missoum, M., Hamidat, A., Imessad, K., Bensalem, S., Khoudja, A. (2016). Impact of a grid-connected PV system application in a bioclimatic house toward the zero energy status in the north of Algeria. Energy and Buildings, 128: 370-383. https://doi.org/10.1016/j.enbuild.2016.07.005

[14] Sommerfeldt, N., Madani, H. (2017). Revisiting the techno-economic analysis process for building-mounted, grid-connected solar photovoltaic systems: Part one–Review. Renewable and Sustainable Energy Reviews, 74: 1379-1393. https://doi.org/10.1016/j.rser.2016.11.232

[15] Chakir, A., Tabaa, M., Moutaouakkil, F., Medromi, H., Alami, K. (2020). Smart multi-level energy management algorithm for grid-connected hybrid renewable energy systems in a micro-grid context. Journal of Renewable and Sustainable Energy, 12(5): 055301. https://doi.org/10.1063/5.0015639

[16] González, A., Riba, J.R., Rius, A. (2015). Optimal sizing of a hybrid grid-connected photovoltaic–wind–biomass power system. Sustainability, 7(9): 12787-12806. https://doi.org/10.3390/su70912787

[17] Falama, R.Z., Kaoutoing, M.D., Mbakop, F.K., Dumbrava, V., et al. (2022). A comparative study based on a techno-environmental-economic analysis of some hybrid grid-connected systems operating under electricity blackouts: A case study in Cameroon. Energy Conversion and Management, 251: 114935. https://doi.org/10.1016/j.enconman.2021.114935

[18] Dalton, G.J., Lockington, D.A., Baldock, T.E. (2009). Feasibility analysis of renewable energy supply options for a grid-connected large hotel. Renewable Energy, 34(4): 955-964. https://doi.org/10.1016/j.renene.2008.08.012

[19] Liu, G., Rasul, M.G., Amanullah, M.T.O., Khan, M.M.K. (2012). Techno-economic simulation and optimization of residential grid-connected PV system for the Queensland climate. Renewable Energy, 45: 146-155. https://doi.org/10.1016/j.renene.2012.02.029

[20] Ramli, M.A., Hiendro, A., Sedraoui, K., Twaha, S. (2015). Optimal sizing of grid-connected photovoltaic energy system in Saudi Arabia. Renewable Energy, 75: 489-495. https://doi.org/10.1016/j.renene.2014.10.028

[21] Gurubel, K.J., Osuna-Enciso, V., Cardenas, J.J., Coronado-Mendoza, A., Perez-Cisneros, M.A., Sanchez, E.N. (2016). Neural forecasting and optimal sizing for hybrid renewable energy systems with grid-connected storage system. Journal of Renewable and Sustainable Energy, 8(4): 045303. https://doi.org/10.1063/1.4960125

[22] González, A., Riba, J.R., Rius, A., Puig, R. (2015). Optimal sizing of a hybrid grid-connected photovoltaic and wind power system. Applied Energy, 154: 752-762. https://doi.org/10.1016/j.apenergy.2015.04.105

[23] Li, J. (2019). Optimal sizing of grid-connected photovoltaic battery systems for residential houses in Australia. Renewable Energy, 136: 1245-1254. https://doi.org/10.1016/j.renene.2018.09.099

[24] Al Garni, H.Z., Awasthi, A., Ramli, M.A. (2018). Optimal design and analysis of grid-connected photovoltaic under different tracking systems using HOMER. Energy Conversion and Management, 155: 42-57. https://doi.org/10.1016/j.enconman.2017.10.090

[25] Ataei, A., Nedaei, M., Rashidi, R., Yoo, C. (2015). Optimum design of an off-grid hybrid renewable energy system for an office building. Journal of Renewable and Sustainable Energy, 7(5): 053123. https://doi.org/10.1063/1.4934659

[26] Fodhil, F., Hamidat, A., Nadjemi, O. (2019). Potential, optimization and sensitivity analysis of photovoltaic–diesel–battery hybrid energy system for rural electrification in Algeria. Energy, 169: 613-624. https://doi.org/10.1016/j.energy.2018.12.049

[27] Khalil, H., Abd El-Hamied, R. (2024). Comparative analysis and assessment of economic profitability of a hybrid renewable energy framework via HOMER optimization in Jordan. International Journal of Heat and Technology, 42: 933-948. https://doi.org/10.18280/ijht.420322

[28] Yimen, N., Monkam, L., Tcheukam-Toko, D., Musa, B., et al. (2022). Optimal design and sensitivity analysis of distributed biomass-based hybrid renewable energy systems for rural electrification: Case study of different photovoltaic/wind/battery-integrated options in Babadam, northern Cameroon. IET Renewable Power Generation, 16(14): 2939-2956. https://doi.org/10.1049/rpg2.12266

[29] Owolabi, A.B., Nsafon, B.E.K., Roh, J.W., Suh, D., Huh, J.S. (2019). Validating the techno-economic and environmental sustainability of solar PV technology in Nigeria using RETScreen Experts to assess its viability. Sustainable Energy Technologies and Assessments, 36: 100542. https://doi.org/10.1016/j.seta.2019.100542

[30] Ganguly, P., Kalam, A., Zayegh, A. (2017). Design an optimum standalone hybrid renewable energy system for a small town at Portland, Victoria using iHOGA. In 2017 Australasian Universities Power Engineering Conference (AUPEC), Melbourne, VIC, Australia, pp. 1-6. https://doi.org/10.1109/AUPEC.2017.8282487

[31] Shamachurn, H. (2021). Optimization of an off-grid domestic hybrid energy system in suburban Paris using iHOGA software. Renewable Energy Focus, 37: 36-49. https://doi.org/10.1016/j.ref.2021.02.004

[32] Shezan, S.A. (2021). Design and demonstration of an islanded hybrid microgrid for an enormous motel with the appropriate solicitation of superfluous energy by using IHOGA and MATLAB. International Journal of Energy Research, 45(4): 5567-5585. https://doi.org/10.1002/er.6184

[33] Caballero, F., Sauma, E., Yanine, F. (2013). Business optimal design of a grid-connected hybrid PV (photovoltaic)-wind energy system without energy storage for an Easter Island's block. Energy, 61: 248-261. https://doi.org/10.1016/j.energy.2013.08.030

[34] Huneke, F., Henkel, J., Benavides González, J.A., Erdmann, G. (2012). Optimisation of hybrid off-grid energy systems by linear programming. Energy, Sustainability and Society, 2(1): 7. https://doi.org/10.1186/2192-0567-2-7

[35] Ashouri, A., Fux, S.S., Benz, M.J., Guzzella, L. (2013). Optimal design and operation of building services using mixed-integer linear programming techniques. Energy, 59: 365-376. https://doi.org/10.1016/j.energy.2013.06.053

[36] Sugimura, M., Gamil, M.M., Akter, H., Krishna, N., Abdel-Akher, M., Mandal, P., Senjyu, T. (2020).

Optimal sizing and operation for microgrid with renewable energy considering two types demand response. Journal of Renewable and Sustainable Energy, 12(6): 065901. https://doi.org/10.1063/5.0008065

[37] Yang, Y., Zhang, S., Xiao, Y. (2017). Optimal design of distributed energy resource systems based on two-stage stochastic programming. Applied Thermal Engineering, 110: 1358-1370. https://doi.org/10.1016/j.applthermaleng.2016.09.049

[38] Zheng, Z., Li, X., Pan, J., Luo, X. (2021). A multi-year two-stage stochastic programming model for optimal design and operation of residential photovoltaic-battery systems. Energy and Buildings, 239: 110835.https://doi.org/10.1016/j.enbuild.2021.110835

[39] Chedid, R., Sawwas, A., Fares, D. (2020). Optimal design of a university campus micro-grid operating under unreliable grid considering PV and battery storage. Energy, 200: 117510. https://doi.org/10.1016/j.energy.2020.117510

[40] Zou, B., Peng, J., Li, S., Li, Y., Yan, J., Yang, H. (2022). Comparative study of the dynamic programming-based and rule-based operation strategies for grid-connected PV-battery systems of office buildings. Applied Energy, 305: 117875. https://doi.org/10.1016/j.apenergy.2021.117875

[41] Akbari, K., Nasiri, M.M., Jolai, F., Ghaderi, S.F. (2014). Optimal investment and unit sizing of distributed energy systems under uncertainty: A robust optimization approach. Energy and Buildings, 85: 275-286. https://doi.org/10.1016/j.enbuild.2014.09.009

[42] Rodríguez-Gallegos, C.D., Yang, D., Gandhi, O., Bieri, M., Reindl, T., Panda, S.K. (2018). A multi-objective and robust optimization approach for sizing and placement of PV and batteries in off-grid systems fully operated by diesel generators: An Indonesian case study. Energy, 160: 410-429. https://doi.org/10.1016/j.energy.2018.06.185

[43] Abadlia, I., Hassaine, L., Beddar, A., Abdoune, F., Bengourina, M.R. (2020). Adaptive fuzzy control with optimization using genetic algorithms for grid-connected hybrid photovoltaic–hydrogen generation systems. International Journal of Hydrogen Energy, 45(43): 22589-22599. https://doi.org/10.1016/j.ijhydene.2020.06.168

[44] Maleki, A., Hafeznia, H., Rosen, M.A., Pourfayaz, F. (2017). Optimization of a grid-connected hybrid solar–wind–hydrogen CHP system for residential applications using efficient metaheuristic approaches. Applied Thermal Engineering, 123: 1263-1277. https://doi.org/10.1016/j.applthermaleng.2017.05.100

[45] Khatib, T., Mohamed, A., Sopian, K. (2012). Optimization of a PV/wind micro-grid for rural housing electrification using a hybrid iterative/genetic algorithm: Case study of Kuala Terengganu, Malaysia. Energy and Buildings, 47: 321-331. https://doi.org/10.1016/j.enbuild.2011.12.006

[46] Bouderres, N., Kerdoun, D., Djellad, A., Chiheb, S., Dekhane, A. (2022). Optimization of fractional order PI controller by PSO algorithm applied to a grid-connected photovoltaic system. Journal Européen des Systèmes Automatisés, 55(4): 427-438. https://doi.org/10.18280/jesa.550401

[47] Ghorbani, N., Kasaeian, A., Toopshekan, A., Bahrami, L., Maghami, A. (2018). Optimizing a hybrid wind–PV–battery system using GA-PSO and MOPSO for cost reduction and reliability enhancement. Energy, 154: 581-591. https://doi.org/10.1016/j.energy.2017.12.057

[48] Miao, D., Hossain, S. (2020). Improved gray wolf optimization algorithm for placement and sizing of electrical energy storage systems in micro-grids. ISA Transactions, 102: 376-387. https://doi.org/10.1016/j.isatra.2020.02.016

[49] Nagadurga, T., Narasimham, P.V.R.L., Vakula, V.S., Devarapalli, R. (2022). Gray wolf optimization-based optimal grid-connected solar photovoltaic system with enhanced power quality features. Concurrency and Computation: Practice and Experience, 34(5): e6696. https://doi.org/10.1002/cpe.6696

[50] Abdulhadi, M.A., Sadeq, M.A., Turki, A.Q. (2025). Cost-effective configuration of hybrid solar–wind energy systems using grey wolf optimization for specified power requirements. Journal Européen des Systèmes Automatisés, 58(3): 623-631. https://doi.org/10.18280/jesa.580318

[51] Mohamed, M.A., Eltamaly, A.M., Alolah, A.I., Hatata, A.Y. (2019). A novel framework-based cuckoo search algorithm for sizing and optimization of grid-independent hybrid renewable energy systems. International Journal of Green Energy, 16(1): 86-100. https://doi.org/10.1080/15435075.2018.1533837

[52] Nadjemi, O., Nacer, T., Hamidat, A., Salhi, H. (2017). Optimal hybrid PV/wind energy system sizing using cuckoo search algorithm: Application to Algerian dairy farms. Renewable and Sustainable Energy Reviews, 70: 1352-1365. https://doi.org/10.1016/j.rser.2016.12.038

[53] Mohamed, A.A., El-Sayed, A., Metwally, H., Selem, S.I. (2020). Grid integration of a photovoltaic system supporting an electric vehicle charging station using SALP swarm optimization. Solar Energy, 205: 170-182. https://doi.org/10.1016/j.solener.2020.05.013

[54] Vahid, M.Z., Hajivand, M., Moshkelgosha, M., Parsa, N., Mansoori, H. (2020). Optimal, reliable and economic design of photovoltaic–wind renewable energy systems considering different storage technologies using improved SALP swarm optimization algorithm. International Journal of Sustainable Energy, 39(5): 465-485. https://doi.org/10.1080/14786451.2020.1716758

[55] Roy, K., Mandal, K.K., Mandal, A.C. (2016). Modeling and management of micro-grid connected systems using improved artificial bee colony algorithm. International Journal of Electrical Power and Energy Systems, 75: 50-58. https://doi.org/10.1016/j.ijepes.2015.08.003

[56] Singh, S., Kaushik, S.C. (2016). Optimal sizing of grid-integrated hybrid PV–biomass energy systems using artificial bee colony algorithm. IET Renewable Power Generation, 10(5): 642-650. https://doi.org/10.1049/iet-rpg.2015.0298

[57] Algabalawy, M.A., Abdelaziz, A.Y., Mekhamer, S.F., Aleem, S.H.A. (2018). Considerations on optimal design of hybrid power generation systems using whale and sine cosine optimization algorithms. Journal of Electrical Systems and Information Technology, 5(3): 312-325. https://doi.org/10.1016/j.jesit.2018.03.004

[58] Zamee, M.A., Won, D. (2020). Novel mode adaptive artificial neural network for dynamic learning: Application in renewable energy sources power generation prediction. Energies, 13(23): 6405. https://doi.org/10.3390/en13236405

[59] Arumugham, V., Ghanimi, H.M., Pustokhin, D.A., Pustokhina, I.V., et al. (2023). An artificial-intelligence-based renewable energy prediction program for demand-side management in smart grids. Sustainability, 15(6):5453. https://doi.org/10.3390/su15065453

[60] Pawar, P., TarunKumar, M. (2020). An IoT based intelligent smart energy management system with accurate forecasting and load strategy for renewable generation. Measurement, 152: 107187. https://doi.org/10.1016/j.measurement.2019.107187

[61] Chia, Y.Y., Lee, L.H., Shafiabady, N., Isa, D. (2015). A load predictive energy management system for supercapacitor-battery hybrid energy storage system in solar application using the Support Vector Machine. Applied Energy, 137: 588-602. https://doi.org/10.1016/j.apenergy.2014.09.026

[62] Mamodiya, U., Kishor, I., Awad, M.M. (2025). A reinforcement learning approach for adaptive energy management. In Proceedings of the 2025 International Conference on Future Telecommunications and Artificial Intelligence (IC-FTAI), Alexandria, Egypt, pp. 1-6. https://doi.org/10.1109/IC-FTAI67960.2025.11384146

[63] Sathishkumar, D., Karthikeyan, C. (2020). Adaptive power management strategy-based optimization and estimation of a renewable energy storage system in stand-alone microgrid with machine learning and data monitoring. International Journal of Wavelets, Multiresolution and Information Processing, 18(1): 1941023. https://doi.org/10.1142/S0219691319410236

[64] Piderit, M.B., Vivanco, F., Van Moeseke, G., Attia, S. (2019). Net zero buildings: A framework for integrated policy development in Chile. Sustainability, 11(5): 1494. https://doi.org/10.3390/su11051494

[65] Ahmed, A., Ge, T., Peng, J., Yan, W.C., Tee, B.T., You, S. (2022). Assessment of renewable energy generation towards net-zero energy buildings: A review. Energy and Buildings, 256: 111755. https://doi.org/10.1016/j.enbuild.2021.111755

[66] Krarti, M., Ihm, P. (2016). Evaluation of net-zero energy residential buildings in the MENA region. Sustainable Cities and Society, 22: 116-125. https://doi.org/10.1016/j.scs.2016.02.007

[67] Tumminia, G., Guarino, F., Longo, S., Aloisio, D., et al. (2020). Grid interaction and environmental impact of a net-zero energy building. Energy Conversion and Management, 203: 112228. https://doi.org/10.1016/j.enconman.2019.112228

[68] Wu, W., Skye, H.M. (2021). Residential net-zero energy buildings: Review and perspectives. Renewable and Sustainable Energy Reviews, 142: 110859. https://doi.org/10.1016/j.rser.2021.110859

[69] Mokhtari, F., Loukarfi, L., Chikhi, M., Imessad, K., Ait Messaoudene, N. (2017). Passive wall design to minimize indoor temperature fluctuations under Algerian Saharan climate. Science and Technology for the Built Environment, 23(7): 1142-1150. https://doi.org/10.1080/23744731.2016.1273020

[70] Nabil, M., Labidine, M.Z. (2022). Application efficiency measures through TRNSYS software on Algerian building to save energy. Journal of Advanced Research in Fluid Mechanics and Thermal Sciences, 93(2): 160-172. https://doi.org/10.37934/arfmts.93.2.160172

[71] Sotehi, O., Chaker, A., Maalouf, C. (2016). Hybrid PV/T water solar collector for net-zero energy buildings and freshwater production: A theoretical approach. Desalination, 385: 1-11. https://doi.org/10.1016/j.desal.2016.01.034

[72] Ringel, M., Laidi, R., Djenouri, D. (2019). Multiple benefits through smart home energy management solutions—A simulation-based case study of a single-family-house in Algeria and Germany. Energies, 12(8): 1537. https://doi.org/10.3390/en12081537

[73] Laib, I., Hamidat, A., Haddadi, M., Ramzan, N., Olabi, A.G. (2018). Study and simulation of the energy performances of a grid-connected PV system supplying a residential house in north of Algeria. Energy, 152: 445-454.https://doi.org/10.1016/j.energy.2018.03.157

[74] Mokhtara, C., Negrou, B., Settou, N., Settou, B., Samy, M.M. (2021). Design optimization of off-grid hybrid renewable energy systems considering building energy performance and climate change: Case study of Algeria. Energy, 219: 119605. https://doi.org/10.1016/j.energy.2020.119605

[75] Benzaama, M.H., Menhoudj, S., Lekhal, M.C., Mokhtari, A., Attia, S. (2021). Multi-objective optimisation of seasonal solar thermal energy storage combined with earth–air heat exchanger for net-zero energy buildings. Solar Energy, 220: 901-913. https://doi.org/10.1016/j.solener.2021.03.070

[76] Khalilpourazari, S., Khalilpourazary, S. (2019). An efficient hybrid algorithm based on water cycle and moth-flame optimization algorithms for solving numerical and constrained engineering optimization problems. Soft Computing, 23(5): 1699-1722. https://doi.org/10.1007/s00500-017-2894-y

[77] Eskandar, H., Sadollah, A., Bahreininejad, A., Hamdi, M. (2012). Water cycle algorithm–A novel metaheuristic optimization method for solving constrained engineering optimization problems. Computers & Structures, 110: 151-166. https://doi.org/10.1016/j.compstruc.2012.07.010

[78] Fodhil, F., Hamidat, A., Nadjemi, O., Alliche, Z., Berkani, L. (2019). Optimum design of a hybrid photovoltaic/diesel/battery/system using water cycle algorithm. In 2019 International Conference in Artificial Intelligence in Renewable Energetic Systems, Bechar, Algeria, pp. 82-93. https://doi.org/10.1007/978-3-030-37207-1_9

[79] Sadollah, A., Eskandar, H., Lee, H.M., Yoo, D.G., Kim, J.H. (2016). Water cycle algorithm: A detailed standard code. SoftwareX, 5: 37-43. https://doi.org/10.1016/j.softx.2016.03.001

[80] Mirjalili, S. (2015). Moth-flame optimization algorithm: A novel nature-inspired heuristic paradigm. Knowledge-Based Systems, 89: 228-249. https://doi.org/10.1016/j.knosys.2015.07.006

[81] Sahoo, S.K., Saha, A.K. (2022). A hybrid moth flame optimization algorithm for global optimization. Journal of Bionic Engineering, 19(5): 1522-1543. https://doi.org/10.1007/s42235-022-00207-y

[82] Fuentes, M., Nofuentes, G., Aguilera, J., Talavera, D.L., Castro, M. (2007). Application and validation of algebraic methods to predict the behaviour of crystalline silicon PV modules in Mediterranean climates. Solar Energy, 81(11): 1396-1408. https://doi.org/10.1016/j.solener.2006.12.008

[83] Li, C., Ge, X., Zheng, Y., Xu, C., Ren, Y., Song, C.,

Yang, C. (2013). Techno-economic feasibility study of autonomous hybrid wind/PV/battery power system for a household in Urumqi, China. Energy, 55: 263-272. https://doi.org/10.1016/j.energy.2013.03.084

[84] Nordin, N.D., Rahman, H.A. (2016). A novel optimization method for designing stand alone photovoltaic system. Renewable Energy, 89: 706-715. https://doi.org/10.1016/j.renene.2015.12.001

[85] Nacer, T., Hamidat, A., Nadjemi, O., Bey, M. (2016). Feasibility study of grid connected photovoltaic system in family farms for electricity generation in rural areas. Renewable Energy, 96: 305-318. https://doi.org/10.1016/j.renene.2016.04.093

[86] Sharafi, M., ElMekkawy, T.Y. (2014). Multi-objective optimal design of hybrid renewable energy systems using PSO-simulation based approach. Renewable Energy, 68: 67-79. https://doi.org/10.1016/j.renene.2014.01.011

[87] Maammeur, H., Hamidat, A., Loukarfi, L., Missoum, M., Abdeladim, K., Nacer, T. (2017). Performance investigation of grid-connected PV systems for family farms: Case study of North-West of Algeria. Renewable and Sustainable Energy Reviews, 78: 1208-1220. https://doi.org/10.1016/j.rser.2017.05.004

[88] Arias, N.B., Franco, J.F., Lavorato, M., Romero, R. (2017). Metaheuristic optimization algorithms for the optimal coordination of plug-in electric vehicle charging in distribution systems with distributed generation. Electric Power Systems Research, 142: 351-361. https://doi.org/10.1016/j.epsr.2016.09.018

[89] Zhang, P., Qian, K., Zhou, C., Stewart, B.G., Hepburn, D.M. (2012). A methodology for optimization of power systems demand due to electric vehicle charging load. IEEE Transactions on Power Systems, 27(3): 1628-1636. https://doi.org/10.1109/TPWRS.2012.2186595

[90] Cai, H., Chen, Q., Guan, Z., Huang, J. (2018). Day-ahead optimal charging/discharging scheduling for electric vehicles in microgrids. Protection and Control of Modern Power Systems, 3(1): 1-15. https://doi.org/10.1186/s41601-018-0083-3

[91] Moon, H., Park, S.Y., Jeong, C., Lee, J. (2018). Forecasting electricity demand of electric vehicles by analyzing consumers' charging patterns. Transportation Research Part D: Transport and Environment, 62: 64-79. https://doi.org/10.1016/j.trd.2018.02.009

NOMENCLATURE

C_I	initial cost, $/kW
C_O	operation and maintenance cost, $/kW
COE	cost of energy, $/kW
C_R	replacements cost, $/kW
CRF	capital recovery factor
Cex	net grid interaction cost, $
D	total number of variables in the system
E_{grid}	annual grid energy, kWh/yr
E_{PV}	E_{PV} annual PV energy, kWh/yr
E_{tot}	annual energy production, kWh/yr
G_{STC}	irradiance under standard test conditions
j	real interest rate
j'	nominal interest rate
LB	lower bounds
MFO	Moth-Flame Optimization algorithm
N	number of replacements for component k
N_P	population size
NPC	net present cost, $
NS_n	number of streams that flow into rivers and the sea
Ns	total count of rivers and a single sea
P_{PV}	PV power, kW
RF	RF Renewable fraction, %
T_a	ambient temperature, ℃
T_{NOCT}	nominal operating cell temperature, ℃
Tp	project duration
T_{STC}	PV cell's operating temperature, ℃
UB	Upper bounds
WCA	Water cycle algorithm

Greek symbols

γ	derating factor
η_{PV}	efficiency of a PV module
η_{inv}	efficiency of an inverter [%]